
















RESEARCH ARTICLE

Shaking table tests of a full-scale flat-bottom manufactured steel silo filled with wheat: Main results on the fixed-base configuration

Stefano Silvestri¹  | Sulyman Mansour²  | Matteo Marra¹  | Johann Distl³  |
 Marco Furinghetti^{4,7}  | Igor Lanese⁴  | Enrique Hernández-Montes⁵  |
 Caterina Neri⁶  | Michele Palermo¹  | Alberto Pavese^{4,7}  |
 Elisa Rizzo Parisi⁴  | Adam Jan Sadowski⁸  | Francesco Selva⁶  |
 Tomoyo Taniguchi⁹  | Laura Vadrucchi⁶  | Felix Weber¹⁰ 

¹ Department DICAM, University of Bologna, Bologna, Italy

² Department DICAR, Technical University of Bari, Bari, Italy

³ Maurer Engineering GmbH, Munich, Germany

⁴ EUCENTRE, Pavia, Italy

⁵ School of Civil Engineers, University of Granada, Granada, Spain

⁶ AGI EMEA Ltd, Ozzano dell'Emilia, Bologna, Italy

⁷ Department DICAR, University of Pavia, Pavia, Italy

⁸ Department of Civil and Environmental Engineering, Imperial College London, London, UK

⁹ Department of Social Systems and Civil Engineering, Tottori University, Tottori, Japan

¹⁰ Maurer Switzerland GmbH, Pfaffhausen, Switzerland

Correspondence

Stefano Silvestri, Department DICAM,
University of Bologna, Bologna, Italy.
Email: stefano.silvestri@unibo.it
 Sulyman Mansour, Department DICAR,
Technical University of Bari, Bari, Italy.
Email: sulyman.mansour@poliba.it

Funding information

H2020 Research Infrastructures,
Grant/Award Number: 730900

[Correction added on May 28, 2022, after
first online publication: CRUI-CARE
funding statement has been added.]

Abstract

This paper reports on a series of shaking table tests on a full-scale flat-bottom steel silo filled with soft wheat, characterized by aspect ratio of around 0.9. The specimen was a 3.64-m diameter and 5.50-m high corrugated-wall cylindrical silo. Multiple sensors were used to monitor the static and dynamic response of the filled silo system, including accelerometers and pressure cells. Numerous unidirectional dynamic tests were performed consisting of random signals, sinusoidal inputs, and both artificial and real earthquake records. The objectives of this paper are (i) to provide a general overview of the whole experimental campaign and (ii) to present selected results obtained for the fixed-base configuration. The measured data were processed to assess the static pressures, the dynamic overpressures (related to the effective mass) and the accelerations of monitored points on the silo wall, and to identify the basic dynamic properties (fundamental frequency of vibration, damping ratio, dynamic amplification factors) of the filled silo. The main findings are discussed and compared with the

This is an open access article under the terms of the [Creative Commons Attribution](https://creativecommons.org/licenses/by/4.0/) License, which permits use, distribution and reproduction in any medium, provided the original work is properly cited.

© 2021 The Authors. *Earthquake Engineering & Structural Dynamics* published by John Wiley & Sons Ltd.

predictions given by available theoretical models and code provisions. It is found that the fundamental frequency slightly decreases with increasing acceleration, while it slightly increases with increasing compaction of the granular material. For close-to-resonance input, the dynamic amplification (in terms of peak values of accelerations) increases along the height of the silo wall up to values of around 1.4 at the top surface of the solid content. The dynamic overpressures appear to increase with depth (differently from the EN1998-4 expectations), and to be proportional to the acceleration.

KEYWORDS

dynamic properties, flat-bottom silo, granular solid, shaking table, pressures

1 | INTRODUCTION

The structural design of steel silos containing granular materials presents a challenging issue.^{1,2} Silos differ from many other civil engineering structures in that the weight of the silo structure is significantly lower than the one of the ensiled granular material and, in case of earthquake ground motion, the particle-structure interaction plays an important role in the global dynamic response. The complex mechanism through which the ensiled material interacts with the silo wall has been studied since the XIX century.^{3–4} Nonetheless, several issues are still to be addressed and structural failures still occur during filling and, especially, discharging phases, as well as during strong ground motions. It is well known that both metal and concrete silos are characterized by a relatively high failure rate (both ground- and columns-supported silos), particularly during earthquakes.⁵

Indeed, during the last century, a number of strong earthquakes provoked catastrophic silo collapse events which incurred extensive economic losses.⁶ After the famous 1999 Chi-Chi earthquake in Taiwan when almost all the silos in a circle of 70 km far from the epicenter collapsed, the EQE report (1999) stated that “the seismic design of practice that is used for the design and construction of such facilities clearly requires a major revision”, thus clearly indicating that actual design procedures have limits.⁷

Current seismic design recommendations for silo structures are often based on approximate assumptions resulting from an incomplete knowledge of the seismic response of real silos due to limited number of experimental investigations. In general, current seismic design procedures provide estimates of the quasi-static horizontal forces generated on the silo wall by the ensiled content based on the concept of an *effective mass*,⁸ defined as the fraction of the total ensiled mass interacting with the silo wall under seismic excitation. For example, EN 1998-4⁸ currently provides two methods (one of which one is considered to be a ‘simplified’ one) for obtaining the global seismic response and the seismic action effects in the supporting structure. The simplified method considers an effective mass equaling 80% of the total ensiled mass, according to the studies of Rotter and Hull⁹ and Younan and Veletsos,^{10–11} that is balanced by the horizontal actions provided by the silo wall. However, there is evidence that for squat or intermediate flat-bottom silos this formulation is too conservative.^{12–13}

With the aim of extending the classical (static) approach proposed by Janssen,^{3–4,8} members of the present research team (Silvestri et al.¹⁴ and Pieraccini et al.¹⁵) proposed an analytical model to evaluate the dynamic actions exerted by an incompressible ensiled content on the wall of a flat-bottom cylindrical container under seismic actions modelled as time-constant horizontal accelerations. For the case of squat flat-bottom silos, the theory predicts quite low values of effective mass. So far, it has been experimentally validated with shaking table tests¹⁶ performed in the Bristol EQUALS lab on a small-scale polycarbonate cylindrical specimen filled (up to two different heights) with Ballottini glass ensiled material considering two values of the particle-wall friction (0.30 and 0.45). The tests were performed on an idealized specimen with the precise purpose of verifying the main assumptions of the proposed theory. The results indicated that, for squat flat-bottom silos, the effective mass is indeed lower than the current EN 1998-4⁸ specification, and that the particle-wall friction coefficient plays an important role in the distribution of the inertia forces. These findings are also consistent with the numerical results obtained by Holler and Meskouris¹⁷ for silos under earthquake excitation. Experimental verification on a full-scale actual steel silo specimen is thus desirable.

In this respect, a wide shaking table experimental campaign on a full-scale ground-supported steel silo filled with soft wheat was executed at the EUCENTRE lab in Pavia (Italy) within the European project “SEismic Response of Actual steel

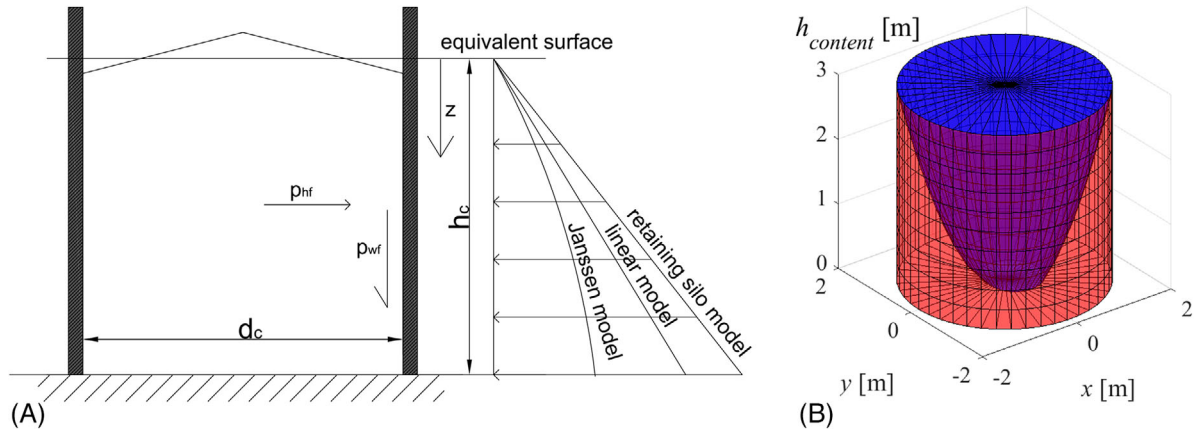


FIGURE 1 (A) Static pressure profiles. (B) Effective mass (red portion) in Silvestri's theory

SILOS (SERA-SILOS)". The main objective of the shaking table tests was to provide new insight into the complex particle-silo interaction under static and dynamic actions (including both harmonic and seismic excitations). In this regard, many issues are still open within the scientific community and still ignored by most of current codes (Section 2). The rationale and a general overview of the whole experimental campaign are provided in Sections 3 and 4, respectively. Then, the main experimental results and first interpretations for the fixed-base configuration are given in Section 5.

2 | ANALYTICAL MODELS AND CURRENT DESIGN METHODS

2.1 | Static design

The well-established Janssen³ (1895) and Koenen⁴ (1896) theory of static pressures exerted by the granular material inside the silo is based upon the full exploitation of the frictional vertical stresses along the particle-wall interface, which enables a portion of the granular solid to be completely sustained by the wall. The provisions of EN 1991-4¹ for symmetrically filled silos are based on this approach. In detail, the horizontal pressure $p_{hf}(z)$ at any depth z below the 'equivalent' surface of the granular solid after filling and during storage is determined as (Figure 1A):

$$p_{hf}(z) = \gamma \cdot K \cdot z_0 \cdot (1 - e^{-z/z_0}) \quad \text{where} \quad z_0 = A / (K \cdot \mu_{GW} \cdot U) \quad (1)$$

where γ is the unit weight, K is the lateral pressure ratio, μ_{GW} is the fully-developed wall friction coefficient between the granular solid and the silo wall, and A and U are the area and the internal perimeter of the plan cross-section of the silo respectively.

This simple equation is an important reference against which many test results and other load models, such as those prescribed for silos with lower aspect ratios^{1,18} (h_c/d_c , where h_c is the height of the ensiled content and d_c is the silo diameter), are often compared. For instance: linear "geostatic" model corresponding to the first two terms of the Taylor series expansion of the Janssen equation, and linear model amplified by a factor depending on the angle of repose, θ_{repose} , of the granular solid, as provided by EN1991-4 for the retaining silos ($h_c/d_c < 0.4$).

2.2 | Current seismic design

In 1983 Trahair et al.¹⁹ proposed the first analytical formulation for predicting the additional distribution of granular material overpressures (relative to filling pressures) on the silo wall under seismic excitation. For slender ground-supported silos, the formula is based on the hypothesis that, when excited by a horizontal acceleration, the whole ensiled material is mobilized. In other words, the *effective mass*,^{8,14,20} defined as the portion of overall ensiled mass horizontally supported by the silo wall during seismic activity, equals the total mass. The unit wall loading exerted by the granular material is assumed as proportional to a constant horizontal acceleration, and uniform with silo height and along the silo circumference, by simply subdividing the total mass volume by the internal surface of the silo wall. For squat ground-supported

silos, the formula accounts for a fraction of the total contained mass. The formulation ignores the vertical particle-wall frictional stress.

Current seismic design standards for ground-supported silo structures qualitatively identify the variables of the physical problem and, when they introduce quantitative formulas, typically do so on the basis of simple assumptions that often lead to overly conservative estimations. ASCE 7–10 (2010)²⁰ provides general principles regarding lateral forces and effective mass but without giving application formulas. It simply states that intergranular friction can transfer seismic shear directly to the foundation and should be considered, that lateral forces should be determined by the requirements and accelerations for short period structures and that the effective mass is related to the characteristics of the product, the aspect ratio, and the seismic intensity. EN 1998-4 provides specific principles and application rules for the seismic design of ground-supported silos, giving formulas for the additional horizontal pressures on the wall during seismic activity which, however, neglect the frictional properties of the granular solid. Barring a more accurate evaluation, the effective mass is assumed as 80% of the total mass of the content (instead of 100%, excluding the base cone portion of the content which is supposed to transfer inertia loads directly to the ground).

2.3 | Improved understanding

In 2012 Silvestri et al.¹⁴ extended Janssen's approach for static vertical loads to the evaluation of dynamic overpressures exerted by the granular solid on the wall of ground-supported silos. The original theory, further refined by Pieraccini et al.¹⁵ in 2015, considers an idealized system of a cylindrical container filled with an incompressible compacted material under idealized dynamic conditions such as a time-constant acceleration input. The formulation accounts for the effects of friction between the granular particles and the wall but ignores the effects of horizontal sliding of granular particles. It predicts that only a part of the ensiled mass (the red annular portion shown in Figure 1B whose thickness increases with depth) produces dynamic overpressures on the wall, while the inertia forces generated in the remaining part (the blue portion in Figure 1B) are transferred directly to the ground through frictional mechanisms inside the granular solid. For squat silos, the theory predicts an effective mass noticeably lower than the total mass.

The application of the theory of Silvestri et al. is limited by some mathematical conditions (see Section 7 of the referenced manuscript)¹⁴:

$$\frac{h_c}{d_c} < \frac{1 - \nu_0 \cdot a_{eh0} \cdot \mu_{GW}}{4 \cdot K \cdot \mu_{GW}}; a_{eh0} < \frac{1}{\nu_0 \cdot \mu_{GW}}; a_{eh0} \leq (1 - |a_{ev0}|) \cdot \min(\mu_{GG}, \mu_{GB}) \quad (2)$$

where: a_{eh0} and a_{ev0} are the constant values of the horizontal and vertical accelerations, respectively; $\nu_0 = 1/(1 + a_{ev0})$; μ_{GW} is the particle-wall friction coefficient (μ_{GW_f} for flat wall, μ_{GW_c} for corrugated wall), μ_{GG} is the internal friction coefficient of the granular particles, μ_{GB} is the friction coefficient between the granular particles and the silo base. The first two conditions are related to the existence of the two portions of the granular material identified in the theory (one transmitting inertia forces through layers of granular material directly down to the silo base and one pushing onto the silo wall, in blue and red in Figure 1B respectively) over the whole height of the granular solid content. The third condition represents the acceleration limit to prevent the horizontal sliding of the granular particles. On the other hand, the theory of Pieraccini et al.¹⁵ removed the aspect ratio limitation (the first condition), thus extending the range of validity of the refined theory to any silo configuration (i.e., including both squat and slender silos). However, it kept the horizontal acceleration limits (the second and the third conditions).

No well-established prediction formulas are currently available for the dynamic properties of a filled silo system. However, Younan and Veletsos^{10–11} studied the dynamic response of vertical, rigid and flexible circular cylindrical tanks filled with a homogeneous, linear viscous-elastic solid medium as a continuous unconstrained cantilever shear-beam, highlighting that the fundamental frequency of the system mainly depends on the properties of the solid medium, medium-boundary wall interface conditions and silo aspect ratio. Livaoglu and Durmuş²¹ proposed a formula for the estimation of the fundamental frequency of a filled silo system based on a single-degree-of-freedom (SDOF) flexural cantilever beam with top lumped mass but were not able to verify its effectiveness against experimental data. A review of the available research studies^{19–33} further indicates that:

- The properties of the ensiled material influence the dynamic response. In particular, a rough material (with high friction coefficients) typically leads to larger effective mass and equivalent damping ratio (up to 20%²²).

- The type of excitation and the acceleration amplitude (above or below the critical acceleration value, about 0.3 g - 0.5 g depending on the granular solid, which corresponds to an incipient sloshing motion of the upper part of the granular material as solid particles exceed friction and to dilatation effects^{23–24}) significantly affect the natural frequencies. In particular, close-to-resonance harmonic excitation activates a larger portion of mass with respect to white noise and earthquake excitations.
- The type of excitation substantially influences the dynamic amplifications. Excitations at around the resonance frequency cause dynamic amplification factors (i.e. ratios between the acceleration of the filled silo system and the base acceleration) of between 5 and 10,^{22,25} whilst under white noise and typical seismic excitations the dynamic amplification factors are of between 2 and 5.²⁶ Also, at resonance and for acceleration values greater than the critical value, the dynamic amplification factors of the granular material tend to be higher than those of the silo wall, thereby indicating horizontal granular particles sliding.

2.4 | Open issues

In conclusion, the dynamic response of storage structures containing granular material is strongly influenced by the interaction between the ensiled content and the structural elements. This is particularly true for steel silos whose own weight is significantly lower than the weight of the ensiled material. In this regard, the fundamental issues still not completely understood can be summarized in two main aspects:

- the assessment of the *effective mass*, which is related to the *dynamic overpressures* exerted by the granular content on the silo wall;
- the assessment of the *fundamental frequency of vibration*, due to uncertainties concerning the lateral stiffness provided by ensiled material.

Consequently, the main shortcomings of standards relating to the seismic design of silos are summarized here. There are no formulas for a reliable quantitative estimation of the effective mass, the fundamental frequency and the distribution of additional horizontal pressures exerted by the granular material on the silo wall. Most standards generally refer to an effective mass that is, at least, 80% of the overall stored granular mass, regardless of the aspect ratio and the physical characteristics of the bulk solid stored. In general, when estimating a design horizontal acceleration, silos are considered as rigid structures, regardless of aspect ratio and/or manufacturing material.

3 | THE RATIONALE AND THE OBJECTIVES OF THE EXPERIMENTAL CAMPAIGN

An extensive shaking table experimental campaign was developed at the EUCENTRE lab³⁴ in Pavia (Italy) between February and March 2019 on a full-scale flat-bottom manufactured steel silo with stiffened corrugated walls filled with soft wheat, considering both fixed-based and seismically isolated-base conditions. The motivation was to provide an insight into the dynamic and seismic response of real filled silo systems. The experimental results may therefore contribute to the full experimental validation of a long-term research program initiated with the formulation of the simplified analytical model proposed by Silvestri et al.,¹⁴ then first verified through experimental tests on idealized specimens with reduced scale.¹⁶ In this respect, Figure 2 schematically represents the logical framework of the overarching approach (in terms of assumptions and aims) from the development of the simplified analytical model^{14,15} (step A: theory), to the first experimental verification under “idealized conditions¹⁶” (step B: proof of concept), up to the final experimental verification carried out on a real full-scale silo under unidirectional base excitation (step C: theory adequacy validated in simulated environment). Indeed, the experimental study on a real full-scale silo can shed light on various aspects, including: (i) the effects of a real compressible granular solid, (ii) the size/scale of the specimen, (iii) the influence of a corrugated steel wall, and (iv) the dependence of the dynamic response of the filled silo system on the characteristics of the input motions.

In this context, the main objectives of the whole experimental campaign are:

1. the evaluation of the static pressures exerted by the ensiled material onto the silo wall,
2. the identification of the basic dynamic properties (fundamental frequency, damping ratio, dynamic amplification factor) of the filled silo system,

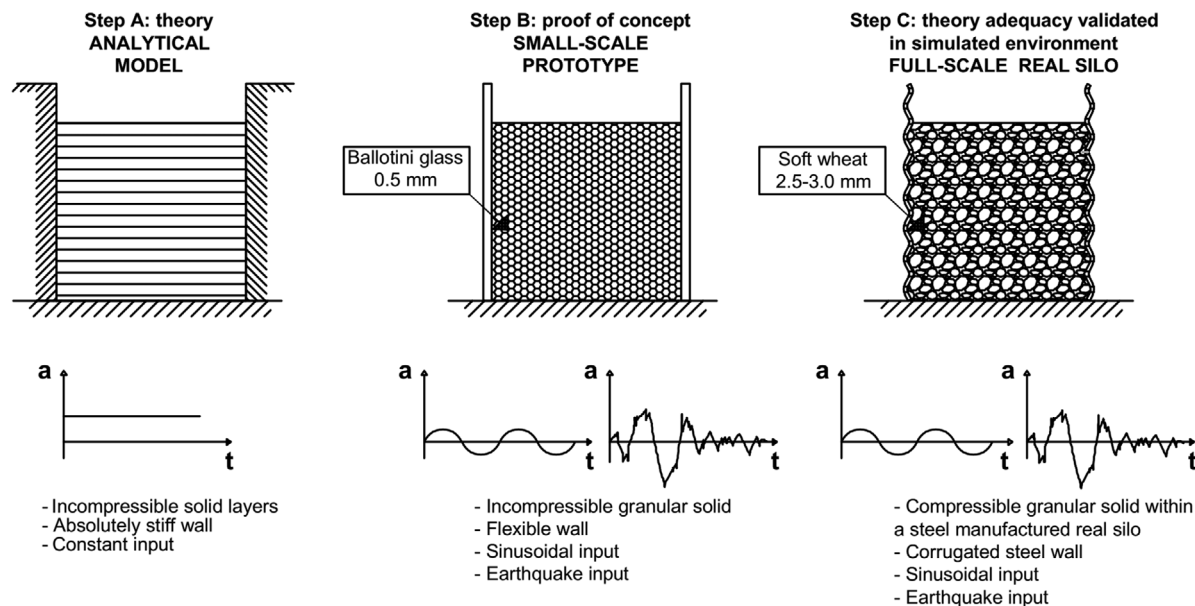


FIGURE 2 Logical framework of the developed research

- the assessment of the dynamic response (in terms of accelerations and dynamic overpressures) exerted by the ensiled material onto the silo wall,
- the validation of Silvestri's and Pieraccini's analytical models in a realistic environment, and
- the assessment of the benefits obtained introducing an isolation system at the base of the silo.

As anticipated in the introduction, this paper focuses on objectives 1, 2, 3 and 4 with reference to the fixed-base configuration. The discussion of the isolated-base configuration (objective 5) is left to a forthcoming specific paper. However, it is worth anticipating here that, as expected, the isolation system significantly mitigates both dynamic overpressures and accelerations on the silo superstructure.

4 | THE EXPERIMENTAL CAMPAIGN

4.1 | The steel silo specimen

A 3.64-m diameter and 5.50-m high flat-bottom steel cylindrical silo specimen (Figure 3) with a corrugated and stiffened wall (small silo selected from a commercial catalog of an Italian manufacturing company) was tested, that could fit the dimensions (5.6 m x 7 m) and the capacity (payload up to 100 t for peak accelerations around 1 g) of the EUCENTRE unidirectional shaking table.

The silo wall was constructed out of 5 strakes of horizontally corrugated curved sheets with thickness equal to 1 mm. Each single sheet had a height of 881 mm and covered one fourth of the silo circumference. Thus, four sheets were bolted together to form a single strake. The vertical joints between the sheets were spaced 2857.5 mm apart and were made up of three rows of M10 (class 8.8, hot galvanized) bolts while the horizontal joints consisted of a single row of M10 bolts (Figure 4). The silo wall was supported by 8 vertical stiffeners characterized by a hat-shaped thin open cross-section which changed in thickness over the height (from the top to the bottom: 1.5 mm for the first strake near the roof, 2 mm for the second and the third strakes, and 3 mm for the last two near the base). The stiffeners were connected to the wall by M10 bolts following a spacing of 67.7 mm equal to the corrugation wavelength. The silo roof consisted of 16 inclined metal sheets.

The wall sheets and stiffeners were made of S350GD steel with Z450 galvanization. The model was built on a 40 cm-thick reinforced concrete (r.c.) foundation plate, already placed on four Curved Surface Sliders friction pendulum isolators³⁵⁻³⁶ that were installed on the shaking table. Steel anchor bolts were used to connect the steel base plates (400 mm x 435 mm x 10 mm, Figure 5A) of the stiffeners to the r.c. plate: six connectors were used for the stiffeners #4 and #8



FIGURE 3 Tested silo: (A) view from above; (B) bolts connecting two overlapping sheets of the silo wall; (C) bolted connection between the vertical stiffeners and the wall; (D) Curved Surface Sliders; (E) r.c. plate

(aligned to the input direction) and #2 and #6 (perpendicular to the input direction), while four connectors were placed at the base of the other stiffeners. Steel ribs were welded at the upper surface of the base plates. All construction details were specifically designed for the test to ensure the elastic structural response of the structure, since the main objective of the test was not to investigate the ductile capacity and the failure mechanisms of the structure, but to get information about the particle-silo interaction. To obtain the fixed-base configuration, stiff steel anchorage devices were placed between the side edges of the r.c. plate and the steel table along the motion direction to avoid any rigid body mechanism such as sliding and rocking/uplift of the system. The weight of the steel silo was found to be 12 kN, the weight of the granular material approximately 285 kN, while that of the $4.8 \text{ m} \times 4.8 \text{ m} \times 0.4 \text{ m}$ r.c. plate approximately 230 kN; leading to a total system weight of 527 kN.

4.2 | The ensiled content: soft wheat

The silo was filled in a moderately eccentric manner up to a height of around 3.3 m with soft wheat to achieve a filled aspect ratio roughly equal to 0.9, corresponding to the squat silo category according to EN1991-4¹. The unit weight of the wheat was measured by means of a classical method (sample of hand compacted granular material put within a well-known

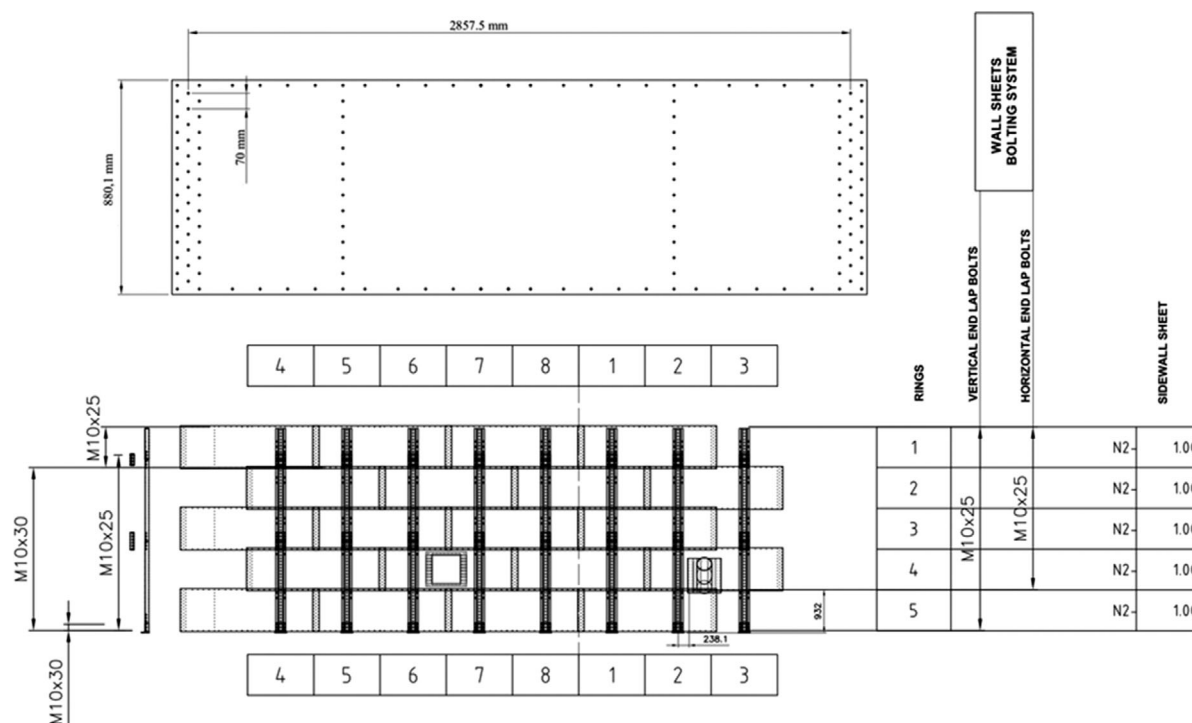


FIGURE 4 Flat development of the silo wall sheets

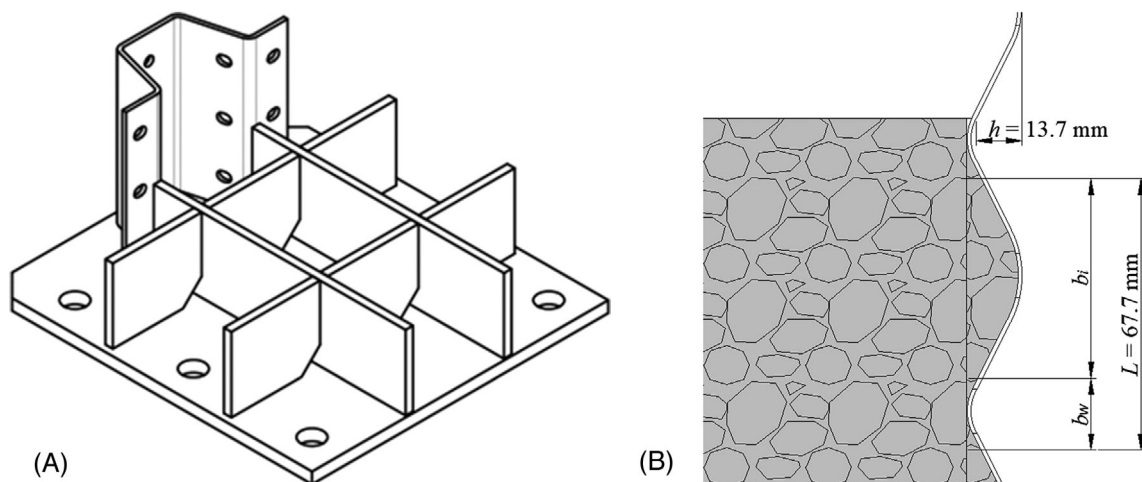
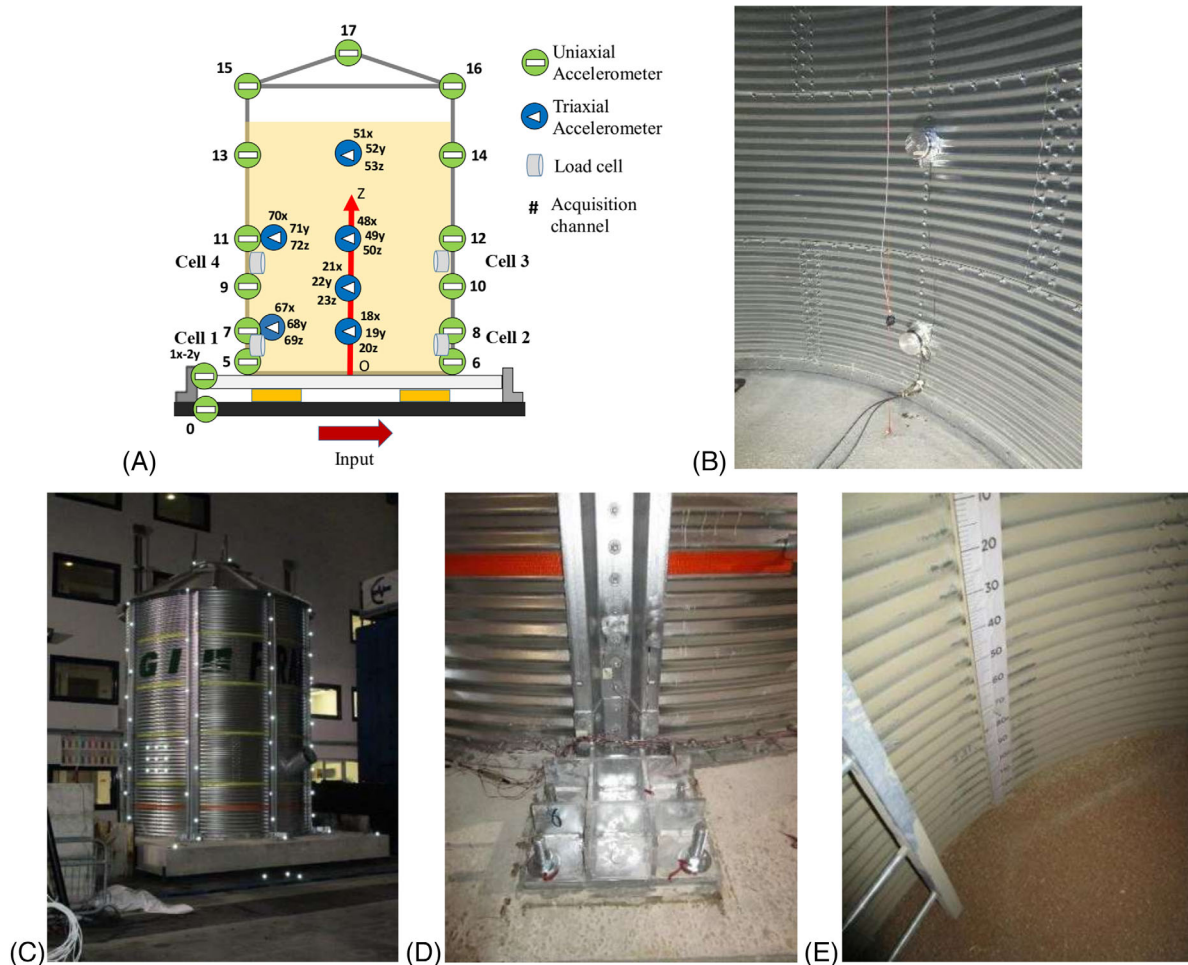


FIGURE 5 (A) 3D sketch of the base plate. (B) Cross-section of the corrugated wall interface with the granular material inside the silo

volume container) and found to be 8.04 kN/m^3 , 8% larger than the lower limit specified by EN1991-4¹ and close to the upper limit assigned by ANSI-ASAE S433.1². Experimental tests were developed following the Annex C of EN1991-4 using samples of the granular solid and the steel of the sheets to identify the internal friction coefficient and the particle-wall friction coefficient. Lateral pressure ratio was assumed according to Table E.1 of EN1991-4. Table 1 reports the measured and the assumed values for the bulk properties of the soft wheat. It is worth noticing that the corrugated wall cross-section detailed in Figure 5b makes the overall interface friction coefficient close to the internal friction coefficient of the wheat and far higher (almost double) than the one in the flat wall case, in accordance with the “averaging formula” given by Annex D of EN1991-4, where the effective friction coefficient of the corrugated wall is identified as a function of the internal friction angle of the content material, the friction coefficient of the flat wall and the geometrical aspects of the corrugation wave. The average diameter of the particles was found to be 2.5 – 3 mm, with no more than 4% of fine material of diameter less than 2 mm based on the result of a particle size distribution test and manual measurements. The shaking table tests

TABLE 1 Bulk properties of soft wheat

Property	Symbols ^{14,1}	Value
unit weight (measured)	γ	8.04 kN/m ³
angle of internal friction (measured)	ϕ_i	28°
internal friction coefficient (measured)	$\mu_{GG}(= \tan \phi_i)$	0.55
flat wall friction coefficient (measured)	$\mu_{GW_f}(= \mu_W)$	0.27
effective corrugated wall friction coefficient (as per Equation (D.1) of EN1991-4 ¹)	$\mu_{GW_c}(= \mu_{eff})$	0.50
base friction coefficient (assumed)	μ_{GB}	0.40 ^{37–38}
lateral pressure ratio (assumed)	K	0.55

**FIGURE 6** (A) Accelerometers and load cells. (B) Load cells. (C) Optical markers. (D) Strain gauges. (E) Graduated bars

were performed in a closed laboratory environment where the air temperature was 16°C and the air humidity was in the range 30% – 45%.

4.3 | Testing instrumentation

Several sensors have been used to monitor the static and dynamic response of the filled silo system, including:

- 15 uniaxial accelerometers, placed at different heights of the silo, to reproduce the acceleration profile and to gain information regarding the dynamic amplification of the filled silo system (Figure 6A);

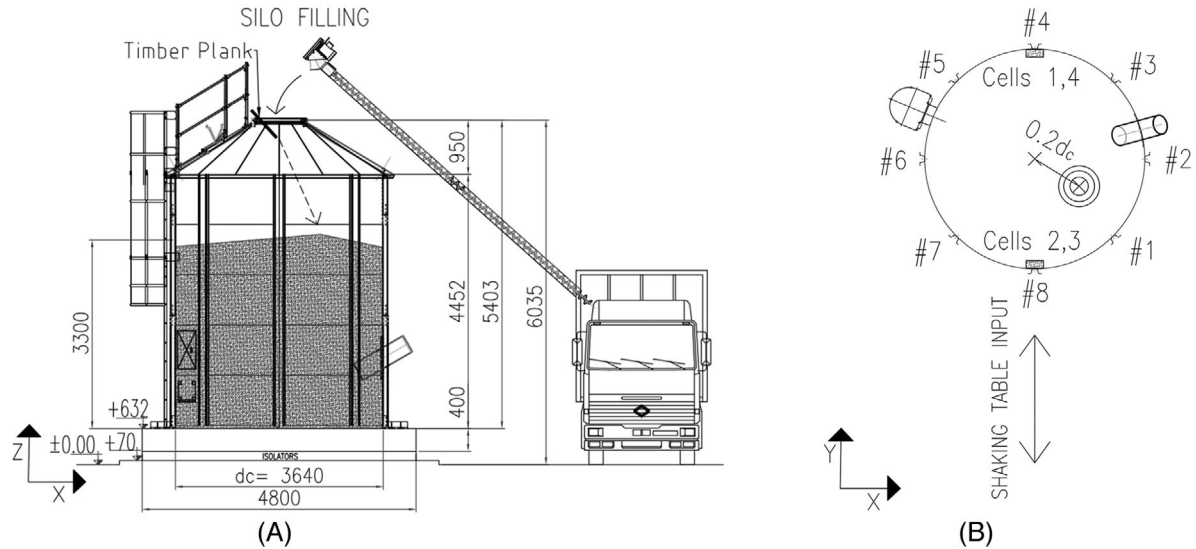


FIGURE 7 (A) Silo filling scheme. (B) Schematic plan view of the asymmetric accumulation of granular material inside the silo

- 6 triaxial accelerometers inside the stored granular solid: 4 placed at different heights in the middle of the solid and 2 close to the internal wall of the silo in correspondence of stiffener #8 (Figure 6A);
- 4 load cells (Figures 6A and B) installed on the internal side of the wall at two heights of the silo near the stiffeners #4 and #8 (the ones aligned to the input motion) in order to measure the horizontal pressures between the granular solid and the wall. Cells 1 and 2 are placed at the base level of 0.42 m above the r.c. plate, while Cells 3 and 4 are placed at the mid-height level of 1.50 m above the r.c. plate;
- 24 strain gauges on the external surfaces of the stiffeners and sheets (Figure 6D);
- 4 vertical graduated bars on the top internal side of the silo to measure the height of granular solid (Figure 6E), to monitor compaction effects;
- 8 LVDT displacement transducers to get the relative motion between the r.c. plate and shaking table (2 horizontal along the input direction, 2 horizontal along the orthogonal direction, and 4 vertical) for the isolated-base case.

In addition, an optical system consisting of 10 high-definition video cameras and 70 optical markers was employed to monitor the displacements of stiffeners #4, #3, #2, #1 and #8, wall, roof, r.c. plate and shaking table (Figure 6E).

4.4 | Filling and discharge

During the 3-hr filling procedure, three trucks entered the lab to fill the silo with a tube connecting the truck storage outlet to the roof opening of the silo (Figure 7A). Filling was performed by slightly deviating the wheat flow with a timber plank, in a moderately eccentric way (Figures 7A and B), as this could affect the position and the functionality of the triaxial accelerometers placed in the middle of the silo. Nevertheless, the eccentricity (around $0.20 d_c$) obtained for the highest point of the top-pile of the granular material (as represented by the center of the small circles in Figure 7B) did not exceed the limit indicated by EN 1991-4¹ for concentric filling conditions in squat or intermediate slenderness silos (namely $0.25 d_c$). The discharge phase was achieved with the aid of an auger inserted through a side tube opening (inclined with an angle of 30° , and placed at the second stroke of the silo wall at a height of 1.27 m).

4.5 | Dynamic testing program

Around 145 uniaxial dynamic tests were carried out considering different types of input at the shaking table level, in fixed-based conditions. White-noise random signals were applied to obtain the basic dynamic properties of the filled silo system. Low-frequency (0.5 and 1 Hz) sinusoids were used which allow a long duration for which the acceleration can be reasonably considered constant in time (around the peak of the sinusoid). Furthermore, three earthquake records were

TABLE 2 Summary of shaking table tests in fixed-based conditions

Nominal PTA	Test	Type of Signal	Nominal PTA	Test	Type of Signal
First series of tests - before compaction			Second series of tests - after compaction		
0.07 g	1	random	0.07 g	88-89	random
0.10 g	2-9	sin 0.5 Hz	0.15 g	90-91	random
	10-13	rs1 eqke	0.20 g	92-93	random
	14-16	a1 eqke	0.25 g	94-96	random
	17-19	rs3 eqke	0.10 g	97-101	sin 0.5 Hz
0.15 g	20-21	random	0.20 g	102-106	sin 1 Hz
0.20 g	22-26	sin 1 Hz	0.30 g	107-111	sin 1 Hz
	29-31	rs1 eqke	0.40 g	112-116	sin 1 Hz
	32-34	a1 eqke	0.50 g	117-121	sin 1 Hz
	35-38	rs3 eqke	0.60 g	122	rs3 eqke
	39-40	random		123	rs1 eqke
0.30 g	41-45	sin 1 Hz		124	rs3 eqke
	46-48	rs1 eqke		125	a1 eqke
	49-51	a1 eqke	Third series of tests - 0.1 g multi-frequency sin. input		
	53-55	rs3 eqke	0.10 g	126-129	sin 5 Hz
0.40 g	56-59	sin 1 Hz		130-134	sin 6 Hz
	60-62	rs1 eqke		135-139	sin 7 Hz
	63-66	a1 eqke		140-145	sin 8 Hz
	67-69	rs3 eqke			
0.50 g	71-76	sin 1 Hz			
	77-80	rs1 eqke			
	81-83	a1 eqke			
	84-86	rs3 eqke			

considered: an artificial earthquake record (a1), a real record of Campano Lucano earthquake (Irpinia, Italy, 23/11/1980) identified as a “far-from-resonance frequency content” input for the tested silo (rs1), a second real record of Kalamata earthquake (Greece, 13/09/1986) identified as a “close-to-resonance frequency content” input (rs3). Finally, sinusoidal tests at constant amplitude and increasing frequency were carried out. Table 2 summarizes the entirety of the dynamic testing program on the fixed-based configuration.

The fixed-base testing can be subdivided into three main series: (i) Tests 1–86: “before compaction” tests, (ii) Tests 88–125: “after compaction” tests, (iii) Tests 126–145: 0.1 g multi-frequency sinusoidal input tests. The free surface of the solid was monitored during the tests by a visual method and the four vertical graduated bars. Compaction was defined in terms of levelling and vertical settlement of the top-surface of the granular solid. It was identified to be fully developed at Test 86 (0.5 g rs3 earthquake input), almost corresponding to the value of the internal friction coefficient of approximately 0.55. Note that several dynamic tests characterized by accelerations up to 0.4 g were not sufficient for the compaction to be fully developed. Real silos are not supposed to be subjected to so many severe earthquake ground-motions during their service life. Thus, in general, “before compaction” tests are considered to be more representative of the actual conditions of real silos. In each series of tests, the actual Peak Table Acceleration (PTA) applied to the silo specimen was close to the target nominal one reported in Table 2.

5 | MAIN EXPERIMENTAL RESULTS AND FIRST INTERPRETATIONS

5.1 | Filling and static pressures

In this section, the pressures recorded during filling and the static pressures between the dynamic tests are discussed (objective 1). Figure 8A shows the horizontal pressure values captured by the four load cells during the effective filling

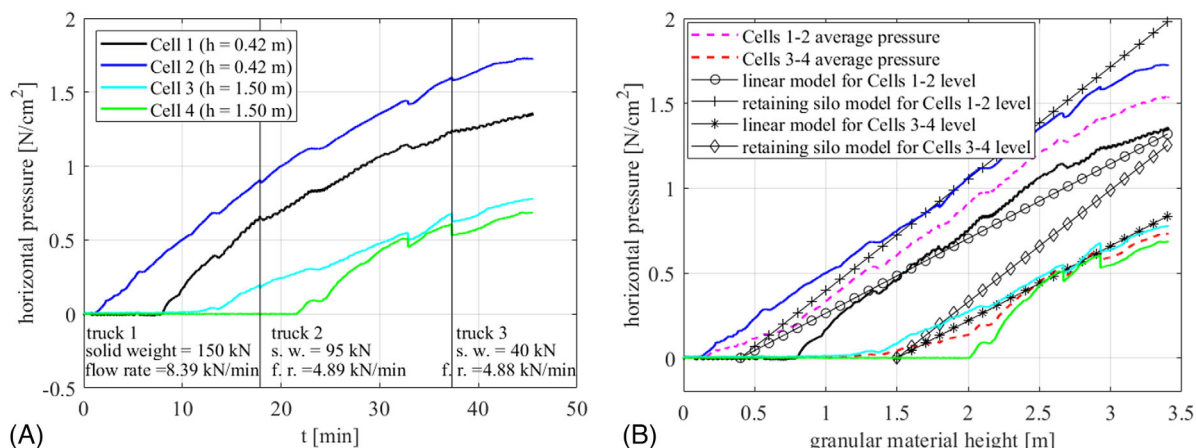


FIGURE 8 (A) Horizontal pressure vs. time during the filling procedure. (B) Horizontal pressure vs. equivalent granular material height during the filling procedure

time. Three trucks were used to transfer the wheat to the laboratory and then to fill the silo. Three hours were required for the whole filling process, including the time needed to set the filling conditions and to change the trucks with the related technical maneuvers. All these dead times were excluded from the registrations since they did not lead to significant changes in the pressure records. Then, starting from the well-known weights of the truck loads (150 kN, 95 kN and 40 kN), the average flow rate was evaluated for each truck. The eccentricity (even if classified “small” with respect to EN1991-4¹) caused by the filling procedure determined a non-synchronous activation of the load cells. At the base level ($h = 42$ cm), Cell 2 became loaded earlier than Cell 1 on the opposite side. The same occurred at the mid-height level ($h = 150$ cm): Cell 3 became loaded before Cell 4.

A further step was conducted to transform the filled amount of granular solid from each truck into an equivalent granular material height on the basis of the plan cross-sectional area of the silo and of each filling time span, assuming a constant value of the flow rate for each truck equal to the calculated average one. Figure 8B thus provides the horizontal pressure values captured by the four load cells as a function of the equivalent granular material height, from which the following observations are made.

From a qualitative point of view, the reconstructed filling profile is increasing almost linearly with the granular material height (i.e., depth z), as it can be clearly read from all cell registrations, except for Cell 4. The small amount of material leaning above the Cell 3 level and thus the small aspect ratio justifies the linear profile. A slight reduction of the slope of the plots is detectable in the second part of the Cell 1 and Cell 2 registrations, which is consistent with the Janssen’s model expectation adopted by EN 1991-4 for larger aspect ratios.³⁹ Cell 4 deviates from all theoretical expectations since it may suffer from combined effects of a significant distance from the peak of the top pile created due to the moderately eccentric filling and a small amount of granular solid leaning above its level.

From a quantitative point of view, assuming constant values of the particle-wall friction coefficient and pressure ratio as reported in Table 1, the average pressure profile at a height of 0.42 m from silo base, corresponding to Cells 1 and 2 level, seems to be within the range identified by the linear (“geostatic”) model and the retaining silo case expectation (linear profile amplified with a function of the repose angle). This is justified by the primary filling conditions experienced by the two cells, which correspond to the retaining silo conditions up to a filling height of roughly 2 m (corresponding to an aspect ratio equal to $(2-0.42)/3.64 = 0.43$). The aspect ratio corresponding to the final configuration (equal to $(3.3-0.42)/3.64 = 0.79$) justifies the final slope reduction. The average pressure profile at a height of 1.50 m from silo base, corresponding to Cells 3 and 4 level, is very close to the linear one, which is plausible due to the small aspect ratio (equal to $(3.3-1.5)/3.64 = 0.49$) of the granular solid leaning above the Cells 3 and 4 level.

During the entire experimental campaign (from the filling day, up to the final day of the tests), it was possible to record the static pressures produced by the granular solid on the silo wall at four locations. Figure 9 displays the static pressure values as captured by the four load cells before each individual test, together with the pressure values estimated by both linear and Janssen models for the two levels.

As it could also be noticed by Figure 8A, the (initial, with respect to dynamic testing) values of the static pressures at the end of the filling day are not symmetrical (Cells 2 and 3 registered larger values than Cells 1 and 4, respectively) due to moderate eccentricities during filling. The dynamic tests started after 5 days, during which Cell 2 recorded an increase

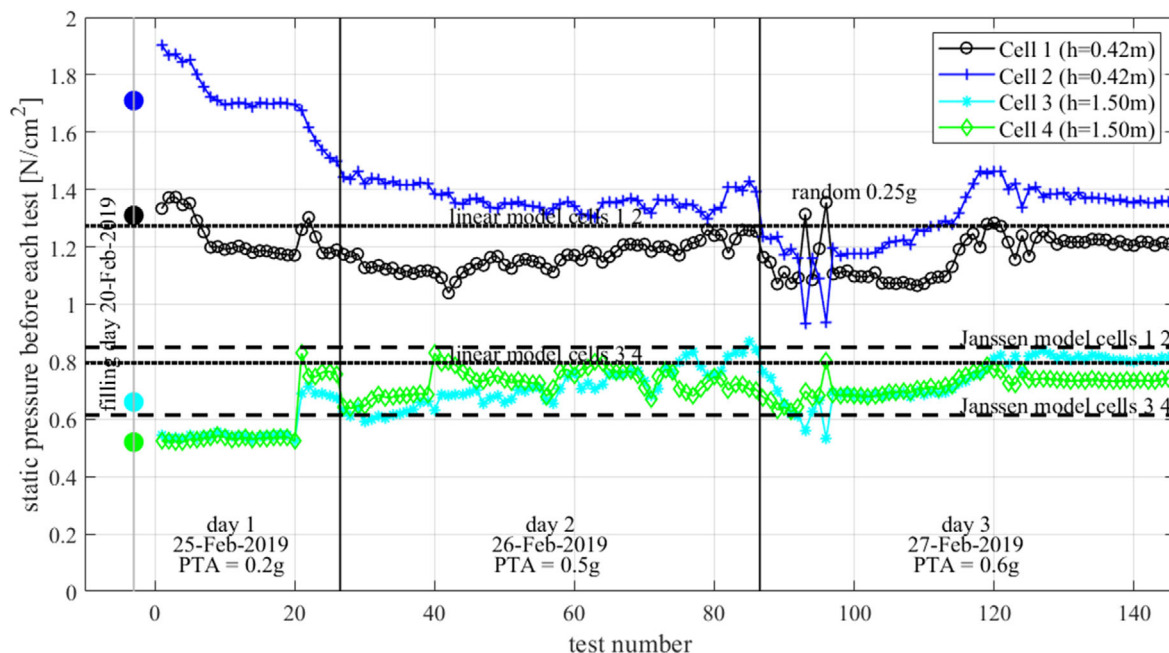


FIGURE 9 Static pressure values as recorded by the four load cells before each single dynamic test

in pressure while Cell 3 recorded a decrease, whilst Cells 1 and 4 showed no significant changes. These variations are due to unascertainable adjustments that may have been occurred inside the granular solid.

During the dynamic tests of the first day (due to levelling phenomena), Cells 1 and 2 at the lower level tended to gradually reach similar values, close to the linear pressure model prediction: $p_{h,1-2} = K \cdot \gamma \cdot z_{1-2} = 0.55 \cdot 8040 \text{ N/m}^3 \cdot 2.88 \text{ m} = 1.27 \text{ N/cm}^2$. Cells 3 and 4 at the higher level recorded similar pressure values, that suddenly increased due to the 0.15 g random Tests 20 and 21 (strong effect of the first significant vertical settlement and compaction of the higher portion of the granular material), tending to the linear pressure model prediction: $p_{h,3-4} = K \cdot \gamma \cdot z_{3-4} = 0.55 \cdot 8040 \text{ N/m}^3 \cdot 1.80 \text{ m} = 0.79 \text{ N/cm}^2$.

In the second and third day, no substantial changes of static pressures (i.e., testing condition) have been provoked by the repeated input, except from the dramatic changes observed after high-intensity random vibration inputs. Indeed, 0.20 g and 0.25 g random Tests 93 and 96 were able to switch the maximum pressure from one side to the other side of the silo.

5.2 | Dynamic identification

The experimental fundamental frequencies of vibration were obtained from the acceleration response of the filled silo system subjected to white-noise random signals for various peak acceleration levels (objective 2). The sampling frequency of the acquired measurements during dynamic testing was 256 Hz and the number of samples in each random record was about 40,000 data points. Raw data was low pass filtered (cutting off at 100 Hz) to remove any offset and drift due to accelerometer noise (typically at high frequencies).

The system transfer function was obtained as the square root of the ratio of the periodogram (which is an estimate of the Power Spectral Density using the Welch method with 50%-overlapping Hamming windows, each one including 1024 samples to obtain a frequency spacing of 0.25 Hz⁴⁰) of the acceleration signal registered at a given level divided by the periodogram of the table acceleration signal. Table 3 summarizes the values of the fundamental frequencies as computed both before and after compaction of the granular solid. It may be seen that the fundamental frequency of the system depends on both the acceleration and the compaction level: it slightly decreases with increasing acceleration (possibly due to slightly larger effective mass; strain-gauges results testified the elastic behavior of the steel structures) and it slightly increases with increasing compaction (higher stiffness provided by granular material).

Illustrative plots of the estimate of the Power Spectral Density of the input signal (accelerometer n. 1 on the r.c. plate) and of the output signal (accelerometer n. 13 on the stiffener at height 2.85 m) are reported in Figure 10a, as obtained for

TABLE 3 Summary of experimental fundamental frequencies

Nominal PTA	First series of tests - before compaction		Second series of tests - after compaction	
	Test	f (Hz)	Test	f (Hz)
0.07 g	1	10.8	88; 89	12.3
0.15 g	20; 21	10.0	90; 91	11.3
0.20 g	39; 40	10.3	92; 93	10.7
0.25 g	–	–	94; 95; 96	10.7

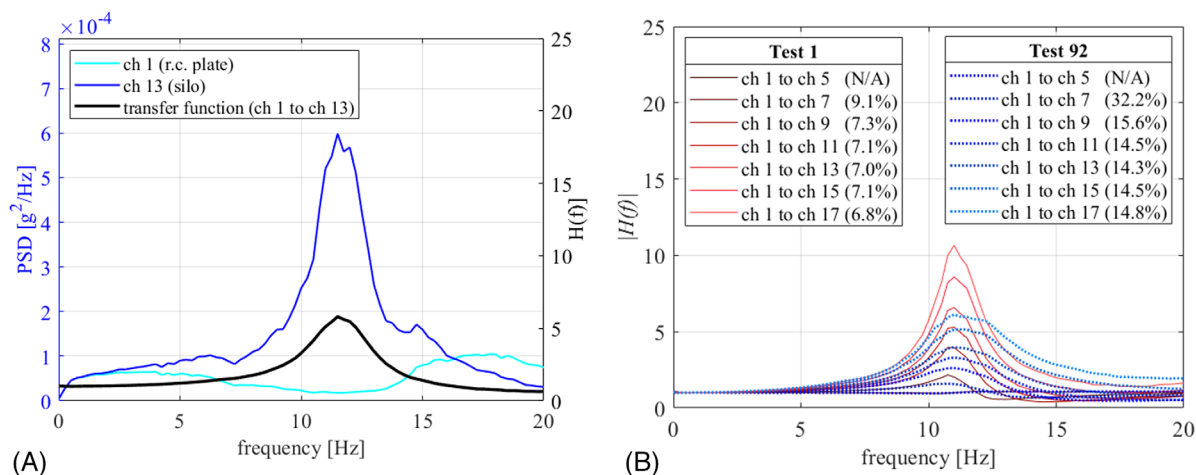


FIGURE 10 (A) PSD estimate and the transfer function of the filled silo system, as obtained for Test 91 (0.15 g random). (B) Transfer functions of the filled silo system, as obtained for Test 1 (0.1 g random) and Test 92 (0.2 g random)

the 0.15 g random input test (Tests 90–91). The same figure also shows the square root of their ratio, i.e. the modulus of the transfer function of the silo.

In the 0–20 Hz frequency range, the shape of the transfer function amplitude is characterized by one peak and thus qualitatively similar to that of a damped SDOF model. Consequently, for preliminary design purposes, the SDOF assumption is considered effective for the filled silo system (generalized SDOF system concept⁴¹).

It is then possible to systematically obtain the transfer functions of the system at different heights in order to gain information about the overall dynamic behavior. Figure 10B, obtained for random Tests 1 and 92, indicates that the amplitude peak of each transfer function occurs always for the same frequency (around 11 Hz), thus confirming the suitability of the generalized SDOF model. An indication of the damping ratio is then inferred by applying the half-power bandwidth method to the moduli of these transfer functions. The obtained damping ratio values are reported in the legend of Figure 10B. They are similar to each other beyond a certain height (i.e., for all accelerometers placed above a certain level). A cautionary note has to be added here, since the damping ratios significantly diverge for the accelerometers close to the silo base, thus making this conclusion about SDOF model suitability limited to accelerometers placed above a given height (channels 11, 12, ..., 17; channel 13, corresponding to the accelerometer close to the top surface of the granular solid, is considered as reference point for the values collected in Figure 11); and further studies are currently under development. Furthermore, the figure suggests that the dynamic amplification increases along the height of the silo (related to the first modal shape of the filled silo system, as better illustrated in the next section) and decreases with the input acceleration level, due to a simultaneous increase in the damping ratio.

With reference to the upper accelerometer (channel 13 of Figure 6A), Figures 11A and B provide the fundamental frequency and the damping ratio (obtained by applying the half-power bandwidth method to the transfer functions) as functions of the actual Peak Table Acceleration. The higher the input acceleration, the higher the equivalent damping ratio, possibly due to enhanced frictional dissipative mechanisms associated to relative sliding of granular particles. The frequency slightly decreases with the input acceleration as consequence of not only the increasing of the damping ratio (however not sufficient to fully explain the observed reduction), but also due to slightly larger effective mass (as also predicted by Silvestri's theory). Linear regression equations are provided for both parameters with the

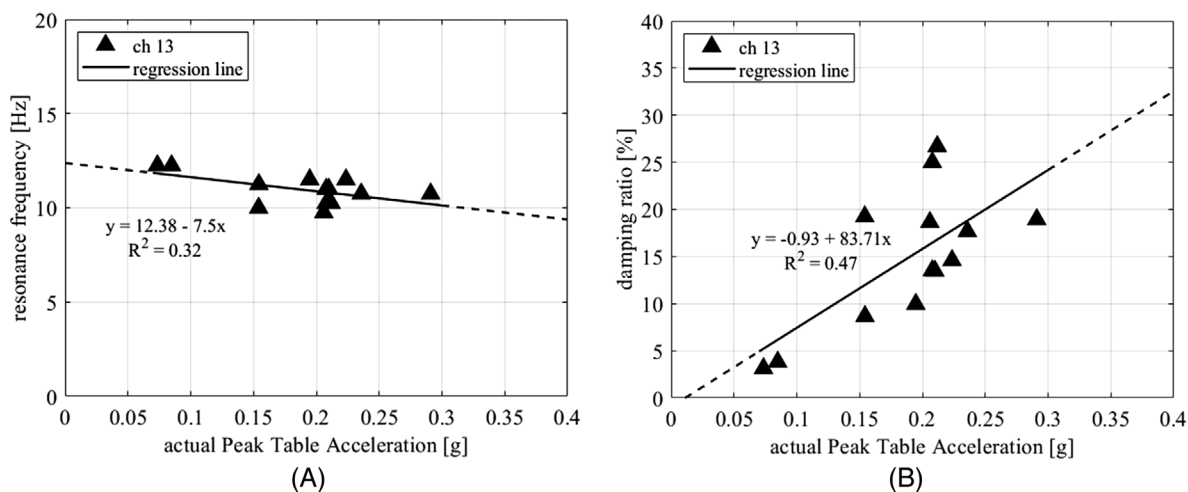


FIGURE 11 For the channel 13 accelerometer: (A) fundamental frequency vs actual PTA and (B) damping ratio vs actual PTA, for random input

following range of applicability: 0.07 g - 0.30 g (solid lines). Extrapolation (dashed lines) is not verified by experimental results.

5.3 | Dynamic response

In this section, selected measured data (accelerations on the silo wall and in the granular solid, dynamic overpressures captured by the four load cells) are presented to give a full picture of the overall dynamic response of the filled silo system (objective 3). Figures 12A, C, E and B, D, F, display the vertical profiles of the peak horizontal accelerations as measured by the uniaxial accelerometers placed at different heights of the silo (on the r.c. plate, along the stiffeners and at the roof top) and by the triaxial accelerometers inside the granular solid, respectively. Both absolute and normalized (with respect to the silo base level, i.e., dynamic amplification factors) acceleration values are provided. In this respect, the vertical profile of the dynamic amplification factors represents an approximation of the first modal shape of the filled silo system, according to the suitability of the generalized SDOF model (as discussed in the previous section). Since the filled silo system is non-linear, the modal shape depends both on the type of input and on the acceleration level. The profiles are given for various inputs: Figures 12A-B refer to 1 Hz sinusoidal input characterized by increasing PTA, Figures 12C-D to the rs3 earthquake input with increasing PTA, and Figures 12E-F to 0.1 g sinusoidal input characterized by increasing frequency. To obtain the acceleration values along the input direction for the triaxial accelerometers that could have achieved random orientation inside the content during the filling process, since they had to be kept free to move together with the granular material, the following assumption was made: no vertical and no transversal components of the system acceleration for an only longitudinal base input acceleration. For each triaxial accelerometer, a single lateral acceleration record (parallel to the input direction) was obtained by applying the square root rule to the three record components, which represents an upper bound of the horizontal acceleration felt by the granular solid.

For the (far-from-resonance) 1 Hz sinusoidal input, the response of the whole system (both the silo wall and the granular material) does not appear to be substantially affected by any dynamic amplification, thus providing results comparable with the Trahair's assumption on uniform acceleration. Just high accelerations are obtained for high-intensity input at the top surface of the granular solid, that could be explained with physical relative movements (similar to sloshing effects) of the loose granular particles (as compared with the underlying more confined layers of granular solid) when the acceleration value (as fraction of g) becomes closer and/or exceeds the internal friction coefficient value. For the (close-to-resonance) rs3 earthquake input, a slight amplification in the silo wall response is observed in the range 1.2 – 1.4 at the granular solid top surface level and at the base roof level, while a larger amplification was noticed at the top roof level (increasing up to 1.6). Meanwhile, greater amplifications are obtained for the granular solid which reached values up to 2 near its top surface at Test 86. Intermediate results (between the ones for the far-from-resonance sinusoidal input and the ones for the close-to-resonance earthquake input) are obtained, but not shown in this paper for sake of brevity, for the rs1

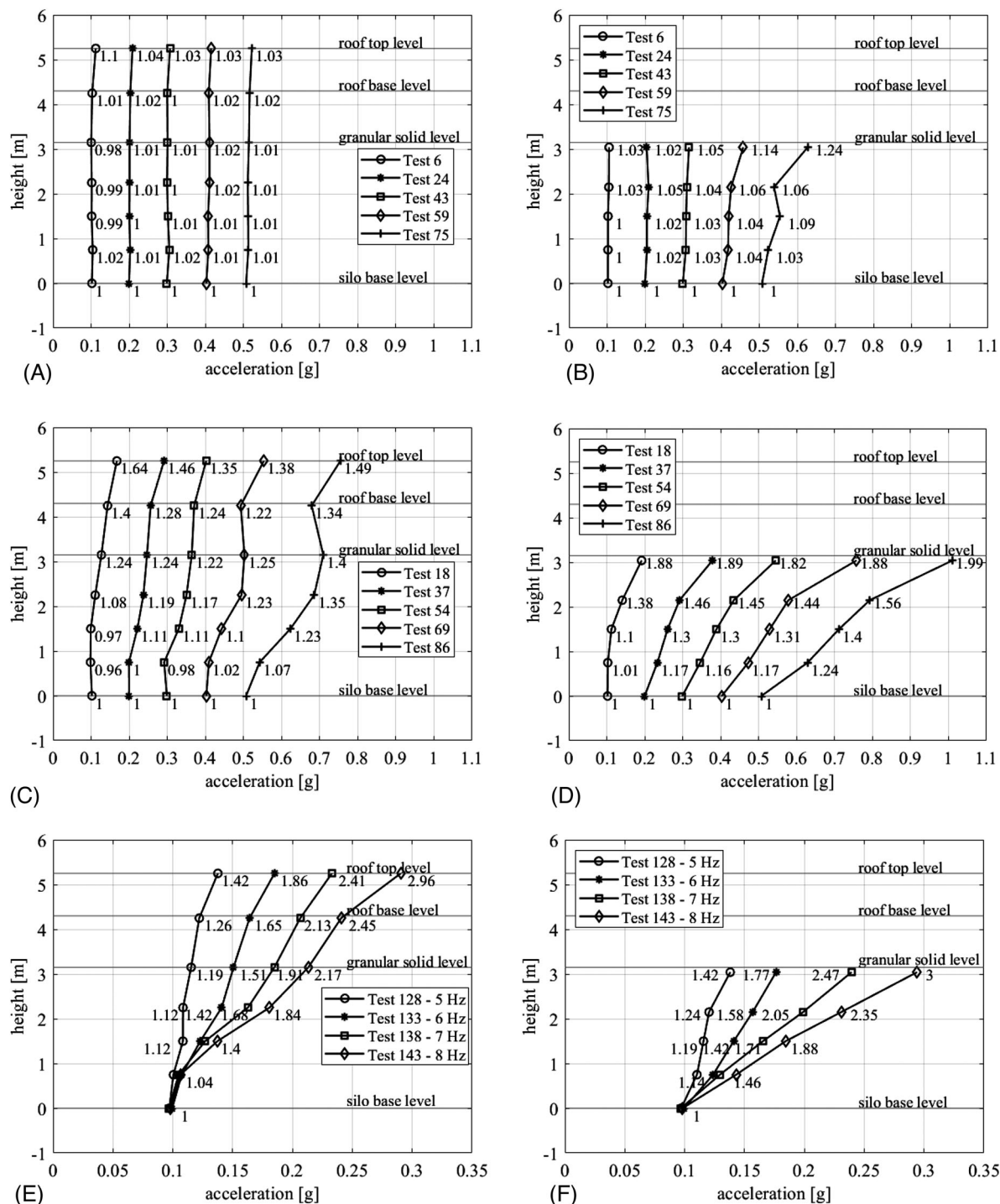


FIGURE 12 Vertical profiles of the peak horizontal accelerations and corresponding dynamic amplification factors for: 1 Hz sinusoidal input (A) along the silo wall and (B) inside the granular material in the middle section, rs3 earthquake input (C) along the silo wall and (D) inside the granular material in the middle section, and for multi-frequency 0.1 g sinusoidal input (E) along the silo wall and (F) inside the granular material in the middle section

and a1 earthquake inputs. Figures 12E-F display the effect of an increasing frequency of the sinusoidal excitation on both the silo wall and the solid content. As expected, the dynamic amplification factor increases by increasing the frequency when approaching the natural frequency of the system up to 2.17 on the silo wall near the granular solid surface and up to 3 in the granular solid at the same level (Test 143).

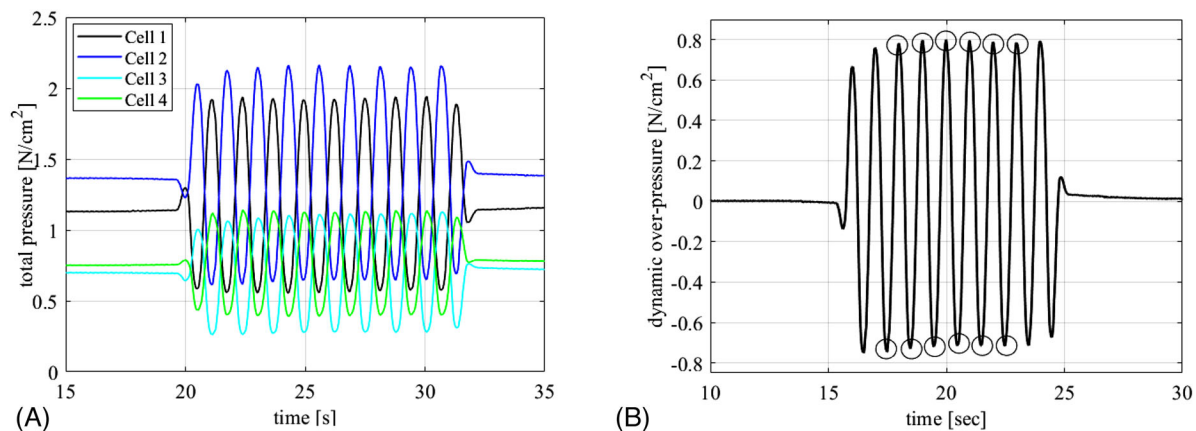


FIGURE 13 (A) Total horizontal pressures measured by the four load cells during Test 45. (B) Illustration of the criterion adopted to assess the reference maximum overpressure value for any sinusoidal test

Regarding the pressure measurements, it is worth pointing out that each pressure cell was specifically designed and mechanically assembled as a horizontal hollow cylinder filled with a moveable aluminum piston that feels the pressure exerted by the granular material on one side and thus pushes against a load cell placed at the base of the hollow cylinder on the other side. The mass of the alloy piston is naturally affected by acceleration and thus produces an additional inertia force that, for sake of accuracy, has to be removed to clean the dynamic overpressure measure from all side effects. Numerically, the piston mass effect was identified test by test, as the product of its volume by the aluminum unit weight (27 kN/m^3) and by the specific acceleration induced in the granular solid at the level of the considered cell, and it reached a maximum value about 0.1 N/cm^2 for the highest acceleration cases.

Figure 13A reports illustrative examples of the data recorded by the pressure cells placed at two levels of the internal surface of the silo wall, during Test 45 (0.3 g 1 Hz sinusoidal input). As expected, the recorded pressure shows a clear sinusoidal trend, providing evidence of the good functioning of the specifically designed load cells. For each test, the dynamic overpressure record is then obtained by subtracting the first value of the record (representative of the static pressure just before the application of the dynamic input) from the total pressure record. Figure 13B shows the dynamic overpressure record of Cell 2 during Test 45 (0.3 g 1 Hz sinusoidal input) and graphically describes the criterion adopted to evaluate the reference maximum overpressure value for any sinusoidal test. It was calculated as the average among the absolute values collected from the peaks of the central cycles (6 out of 10, i.e., excluding the first two introductory and the last two concluding reduced-amplitude cycles). Instead, for any earthquake test, the reference maximum overpressure value was easily evaluated as the maximum absolute one all over the test.

Figure 14 shows the maximum dynamic overpressure divided by the corresponding actual PTA over all tests of the fixed-base configuration. The ordinates thus provide the overpressures due to a unit base acceleration.

In general (except from some deviations in the first and last tests), the response is almost stable. Specifically, this can be clearly noticed for the lower cells in the case of the 1 Hz sinusoidal input tests (highlighted with small red square markers) along all 3 days. From a quantitative point of view, referring - for instance - to the sinusoidal tests of the second testing day, a 0.1 g base acceleration input leads to dynamic overpressures around 2.5 N/cm^2 for the two lower cells (1 and 2) and around 1 N/cm^2 for the two upper cells (3 and 4). Lower values are observed for the initial tests (up to the 0.15 g random tests, i.e. Tests 20 and 21) due to redistribution and adjustments of the granular solid as already noticed in Figure 9. Random inputs (e.g. Tests 39–40) may cause unpredictable deviations of the overpressure/acceleration ratio. An increasing trend is obtained for the last sequence of 0.1 g sinusoidal inputs with increasing frequency (from Test 126 to Test 145), which is consistent with the dynamic amplification response presented in Figures 12E–F.

5.4 | Discussion of the dynamic overpressure profiles

The dependence of the dynamic overpressures on the height of the granular solid (depth z , as measured from top surface downwards) and the acceleration is discussed in this section, and a comparison with the results provided by the three analytical models mentioned in Sections 2.2 and 2.3 is provided (objective 4). Such a problem is not well-established in

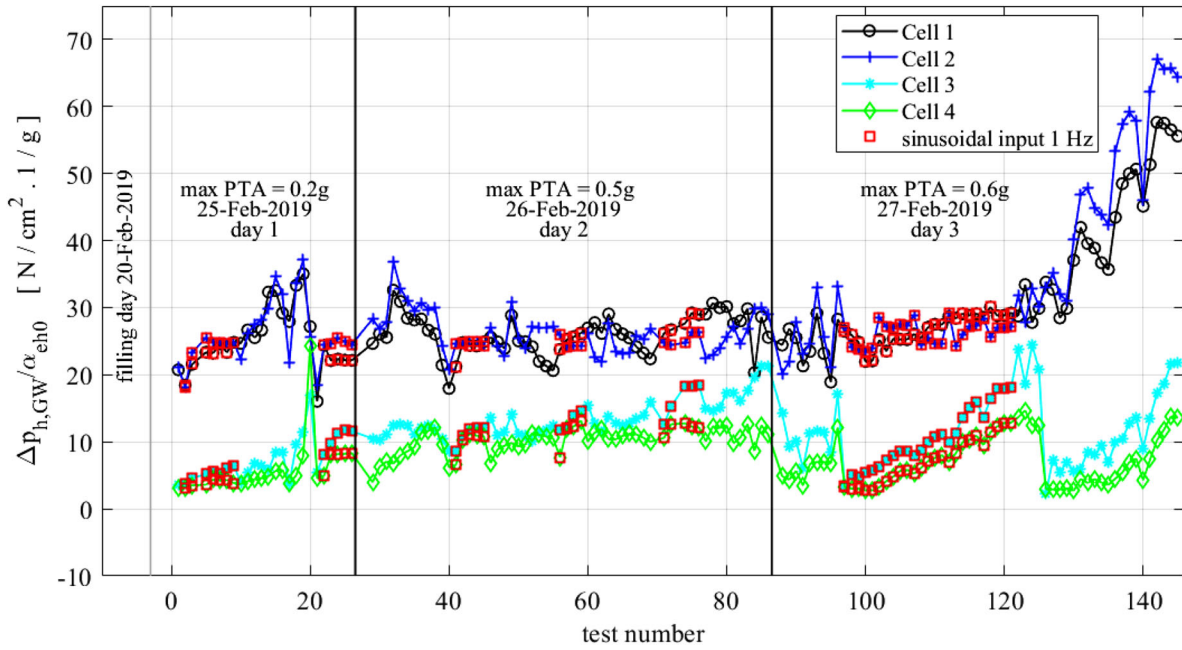


FIGURE 14 Dynamic overpressure/base acceleration ratio for each single test of the fixed-base configuration

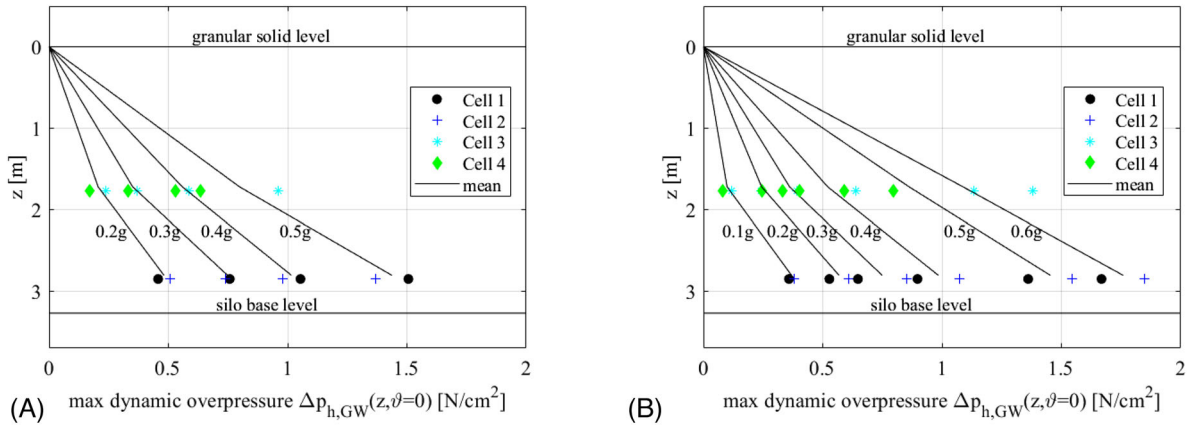


FIGURE 15 Maximum horizontal pressures measured by the four pressure cells for various (A) sinusoidal and (B) earthquake tests

the literature, mainly to the uncertainties related to the measurement of local pressure values and the absolute lack of actual experimental comparable data.

Figures 15A–B compare the dynamic overpressures measured at different acceleration levels for the 1 Hz sinusoidal and the rs3 earthquake inputs. For each acceleration level, the black lines connect the mean value of the pressures measured by the two cells at the base level with that of the two cells at mid-height level within the granular solid, and these, in turn, with the zero value at the top surface of the granular solid. The measured overpressure values increase from the upper to the lower cells (differently from the EN1998-4 expectations). For the sinusoidal case (Figure 15A), the trend is qualitatively consistent with Silvestri's model that, however, is not applicable to the entire tested silo (the aspect ratio limitation given by Equation (2) is not satisfied). On the other hand, the general trend of the overpressure profiles is not in agreement with the along-the-height uniform prediction of Trahair's model, since the acceleration profile is uniform (as per Figures 12A–B, that are consistent with Trahair's assumption). For the close-to-resonance earthquake case (Figure 15B), similar results are obtained; for the upper cells level, a slightly larger dynamic overpressures are observed due to larger accelerations at the same level (as per Figures 12C–D).

For all the 1 Hz sinusoidal input tests before compaction (Tests 2–9, 22–26, 41–45, 56–59 and 71–76), Figures 16A compares the trends of the dynamic overpressures vs. the actual PTA with the predictions of the analytical models available in the

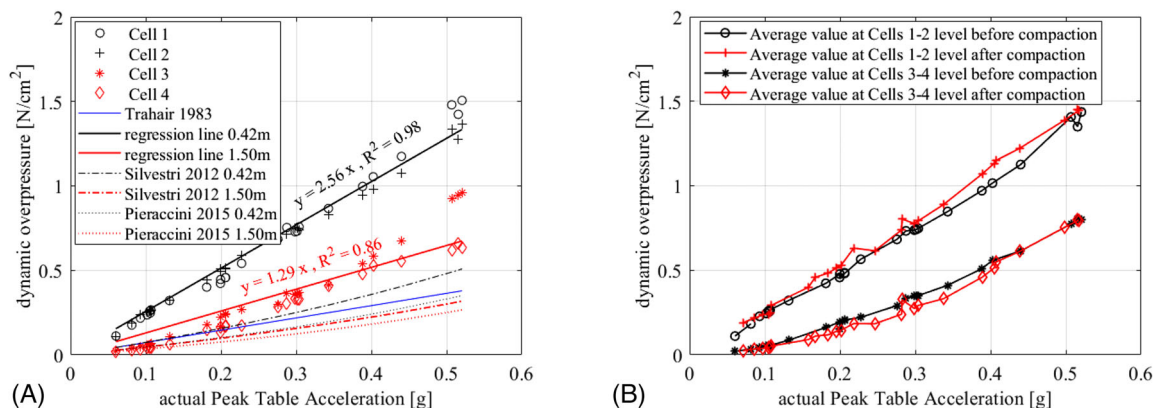


FIGURE 16 Dynamic overpressure vs. actual Peak Table Acceleration for (A) 1 Hz sinusoidal input, (B) 1 Hz sinusoidal input before/after compaction

scientific literature,^{14–15,19} for the two cell levels. Overall, the overpressures show an almost linearly increasing trend with increasing values of PTA. Only for large acceleration values (around 0.5 g, close to the internal friction coefficient value of the granular solid), a small deviation is noticed.

The comparisons shown in Figure 16a reveal that: (i) the trend of the local dynamic overpressures resulted from both the lower (Cells 1 and 2) and the upper (Cells 3 and 4) cells does not agree with any model; (ii) Trahair's model underestimates the results (leading to the same linear equation $y = 0.728x$ for both the lower and the upper cells, where y is the dynamic overpressure, x is the actual PTA and $0.728 \text{ N/cm}^2/\text{g}$ corresponds to the $\gamma \cdot d_c/4$ factor, provided by Trahair for unit acceleration and uniform distribution over the silo height and along the circumference); (iii) Silvestri's model significantly underestimates the lower cells results, while it is able to well capture the upper cells results up to 0.13 g; (iv) Pieraccini's model (which represents, as mentioned in Section 2.3, the updated version of Silvestri's one with extended limits of validity) substantially underestimates the overpressures for both the lower and the upper cells levels; (v) regression lines of the experimental data provide $y = 2.56x$ for the lower cells and $y = 1.29x$ for the upper cells.

These findings indicate that the peak local dynamic overpressures are not captured by design-oriented models based on averaged uniform distributions (such as Trahair's model), and that Silvestri's model can be applied to the portions of the tested silo leaning above certain heights corresponding to aspect ratios smaller than the limit given by Equation (2), depending also on the considered acceleration value. These observations may suggest an interesting interpretation of the dynamic behavior of intermediate/slender silos, that is a complex resisting mechanism resulting in an upper portion of the silo (up to a certain depth from the solid top surface, corresponding to the limit aspect ratio of the first of Equation (2) which behaves according to Silvestri's model (effective mass that can become significantly smaller than the total mass of the ensiled content), and a remaining lower portion of the silo behaving with an effective mass possibly close to the total mass but with alternative overpressures distributions. Nevertheless, additional studies are necessary to confirm this mechanism, leading to possible reformulation of the analytical model.

Figure 16b reports the average values (of the two cells at each level) of the dynamic overpressure values captured from the 1 Hz sinusoidal inputs before (Tests 2–9, 22–26, 41–45, 56–59 and 71–76) and after (Tests 97–121) compaction. No significant effects of the compaction on the dynamic overpressure are detected, since the two plots are very close to each other. However, compaction seems to be slightly increasing and decreasing the overpressures at the base (Cells 1–2 level) and in the middle (Cells 3–4 level) of the granular solid, respectively.

6 | CONCLUSIONS

This paper has presented selected results from a wide experimental campaign aimed at characterizing the dynamic and seismic response of a realistic 5.5 m-high 3.64 m-diameter flat-bottom cylindrical steel silo with a corrugated and stiffened wall under a fixed-base configuration. The silo was filled in a moderately eccentric manner up to 3.3 m height with soft wheat in order to achieve an aspect ratio h_c/d_c of approximately 0.9.

The scientific contribution of the experimental study lies in the realistic nature of the tests performed both in terms of the type of the tested specimen, representative of an actual full-scale steel silo (characterized by corrugated wall,

hat-shaped stiffeners, base connection plates) and filled with a real compressible granular material, and in terms of the applied dynamic excitations, including real earthquake ground motion records. Such a realistic environment allowed to investigate various and still unexplored aspects, such as the actual friction conditions both at the particle-corrugated wall interface and at the product base, and the effect of compaction of the granular solid. Furthermore, the dynamic response of a full-scale filled silo system avoids uncertainties due to scaling issues, since it straightforwardly accounts for the actual weight and equivalent stiffness contribution of the content material, differently from other experimental tests performed on small scaled containers.

The following concluding remarks can be drawn from the experimental campaign:

- Even if slightly disturbed by a moderate eccentricity during the filling process, on average, the recorded horizontal static pressure distribution is qualitatively consistent with the theoretical expectations: linear profile for small aspect ratios (up to $h_c/d_c < 0.4$) and Janssen's model for larger ones.
- During the dynamic tests, compaction of granular solid occurred and redistribution of static pressures between opposite load cells at the same level was observed. Several dynamic tests characterized by accelerations up to 0.4 g were not sufficient to fully develop compaction and to reach an almost horizontal top-surface of the granular solid.
- The damping ratio increases with increasing acceleration (enhanced frictional dissipative mechanisms associated to relative sliding of granular particles), from 5%-10% for 0.05 g-0.1 g random input to 15%-20% for 0.2 g-0.3 g random input.
- The resonance frequency (around 11 Hz) slightly changes according to the characteristics of signal and the conditions of the granular solid. In particular, it slightly decreases with increasing acceleration (increasing of damping ratio and larger effective mass) and it slightly increases with increasing compaction (higher stiffness provided by the granular material).
- No significant dynamic amplification was observed for the whole filled silo system (both the silo wall and the ensiled granular material) for low-frequency sinusoidal inputs. For the most demanding earthquake input (in terms of close-to-resonance frequency content), the dynamic amplification factor increased along the silo wall height up to values around 1.4 at the top surface of the solid content. However, it slightly decreased with increasing acceleration, consistent with an increase in the damping ratio. Larger amplifications were obtained for the internal granular solid, up to 2 near its top surface.
- The measured dynamic overpressures seemed to increase slightly more than linearly with depth from the top to the bottom (differently from the EN1998-4 expectations). They have an almost linear trend with the acceleration, with a slight deviation (increase) for large accelerations corresponding to the range of values of the internal friction coefficient of the granular solid.
- For the upper cells the dynamic overpressure vs. height profile seemed to qualitatively agree with Silvestri's theory (effective mass smaller than the total mass of the filled content), whilst this agreement is not confirmed for the lower cells (violation of the aspect-ratio limit of validity of Silvestri's theory for the investigated silo). Instead, for this latter level, the dynamic overpressure vs. acceleration trend is not captured by design-oriented models and returns large unexpected values for the peak local overpressures that should correspond to distributions other than Trahair's uniform model. These findings can suggest a complex resisting mechanism to be investigated in future research: the upper portion of the silo (up to a certain height) which behaves according to Silvestri's model, and the remaining lower portion of the silo behaving with an effective mass possibly close to the total mass with an enhanced overpressures distribution.

Further detailed interpretation of the data is currently ongoing and will be the object of future publications.

ACKNOWLEDGEMENTS

This project ("SEismic Response of Actual steel SILOS (SERA-SILOS)", <https://sera-ta.eucentre.it/index.php/sera-ta-project-18/>) has received funding from the European Union's Horizon 2020 research and innovation program under grant agreement No 730900. The authors are grateful for this support. Thanks are also due the laboratory personnel at EUCENTRE, Pavia, Italy.

The AGI EMEA S.R.L. (ex AGI FRAME S.R.L.) company (Ozzano dell'Emilia, Bologna, Italy) and the MAURER Engineering GmbH company (Munich, Germany and Pfaffhausen, Switzerland) are thanked for having designed and provided the tested silo and the isolation devices, respectively.

Open Access Funding provided by Politecnico di Bari within the CRUI-CARE Agreement.

DATA AVAILABILITY STATEMENT

The data that support the findings will be made available in a public repository at <https://seradata2euc.eucentre.it/CelestinaDataViewer/projects.xhtml> following an embargo to allow for a wider interpretation by the researchers of the SERA-SILOS project consortium. The intention of the authors is to provide an initial robust scientific production that could serve as a basis for a deep understanding of the experimental campaign, and as a reference to investigate further in detail the results produced.

ORCID

Stefano Silvestri  <https://orcid.org/0000-0003-3587-4114>
 Sulyman Mansour  <https://orcid.org/0000-0001-6416-8564>
 Matteo Marra  <https://orcid.org/0000-0003-3311-5421>
 Marco Furinghetti  <https://orcid.org/0000-0002-7333-1834>
 Igor Lanese  <https://orcid.org/0000-0002-9716-0603>
 Enrique Hernández-Montes  <https://orcid.org/0000-0001-6068-1264>
 Caterina Neri  <https://orcid.org/0000-0001-6489-876X>
 Michele Palermo  <https://orcid.org/0000-0002-1922-1079>
 Alberto Pavese  <https://orcid.org/0000-0003-4616-7693>
 Elisa Rizzo Parisi  <https://orcid.org/0000-0003-0206-1651>
 Adam Jan Sadowski  <https://orcid.org/0000-0003-2099-1895>
 Francesco Selva  <https://orcid.org/0000-0003-2409-4358>
 Tomoyo Taniguchi  <https://orcid.org/0000-0002-9184-6188>
 Laura Vadrucci  <https://orcid.org/0000-0001-5995-2274>
 Felix Weber  <https://orcid.org/0000-0001-6746-6735>

REFERENCES

- EN 1991-4 (2006) *Eurocode 1. Actions on structures, Part 4 -Silos, tanks and pipelines*, CEN, Brussels.
- ANSI/ASAE S433.1 Jan 2019, Loads exerted by free-flowing grain on bins.
- Janssen H. Versuche über Getreidedruck in Silozellen. *Z Ver Dtsch Ing.* 1895;39(35):1045-1049.
- Koenen M, Berechnung des Seiten und Bodendrucks in Silozellen. *Centralblatt der Bauverwaltung*, 1896;16:446-449.
- Rotter JM. *Guide for the Economic Design of Circular Metal Silos*. Spon Press; 2001.
- Dogangun A, Karaca Z, Durmus A, Sezen H. Cause of Damage and Failures in Silo Structures. *Journal of Performance of Constructed Facilities*. 2009;23(2):65-71.
- EQE 1999. "Chichi, Taiwan earthquake of September 21, 1999 M7.6." An EQE Briefing, Jan. 29, 2008.
- EN 1998-4 (2006) *Eurocode 8. Design of structures for earthquake resistance, Part 4 -Silos, tanks and pipelines*, CEN, Brussels.
- Rotter JM, Hull TS. Wall loads in squat steel silos during earthquakes. *Eng Struct*. 1989;11(3):139-147.
- Younan AH, Veletsos AS. Dynamics of solid-containing tanks. I: rigid tanks. *J Struct Eng*. 1998;124(1):52-61.
- Younan AH, Veletsos AS. Dynamics of solid-containing tanks. II: flexible tanks. *J Struct Eng*. 1998;124(1):52-61.
- Dvornik J & Lazarevic D. Loading of granular material on silo walls. In *Processing of the 1st Conference on Applied Mathematics and Computation*, Rogina M, Hari V, Limić N, Tutek Z (eds.): Dubrovnik, Croatia, 1999; pp. 215-222.
- Wagner R, Noh SY, Butenweg C, Meskouris K, Seismic excited granular material silo. In *Proceedings of Eurodyn 2002*, Grundmann & Schueller (eds.) 2002; 253-258. 90 5809510X: pp. 307-333.
- Silvestri S, Gasparini G, Trombetti T, Foti D. On the evaluation of the horizontal forces produced by grain-like material inside silos during earthquakes. *Bulletin of Earthquake Engineering*. 2012;10(5):1535-1560.
- Pieraccini L, Silvestri S, Trombetti T. Refinements to the Silvestri's theory for the evaluation of the seismic actions in flat-bottom silos containing grain-like material. *Bulletin of Earthquake Engineering*. 2015;13(11):3493-3525.
- Silvestri S, Ivorra S, Di Chiacchio L, et al. Shaking table tests of flat-bottom circular silos containing grain-like material. *Earthq Eng Struct Dyn*. 2016;45: 69-89.
- Holler S, Meskouris K. Granular material silos under dynamic excitation: numerical simulation and experimental validation. *J Struct Eng*. 2006;132(10):1573-1579.
- Reimbert M, Reimbert L. *Silos: theory and practice*. *Trans Tech Print*. 1976.
- Trahair NS, Abel A, Ansourian P, Irvine HM, Rotter JM (1983) *Structural design of steel bins for bulk solids*. Australian Institute of Steel Construction, Sydney. 1983; ISBN 0909945357.
- ASCE Standard ASCE/SEI 7-10, Minimum design loads for buildings and other structures, ISBN 978-0-7844-1085-1.
- Livaoglu R, Durmuş A. A simplified approximation for seismic analysis of silo-bulk material system. *Bull Earthq Eng*. 2016;14(3):863-887.

22. Sakai M, Matsumura H, Sasaki M, Nakamura N, Kobayashi M, Kitagawa Y. Study on the dynamic behavior of coal silos against earthquakes. *Bulk Solids Handling*. 1985;5(5):1021.
23. Metcalfe G, Tennakoon SGK, Kondic L, Schaeffer DG, Behringer RP. Granular friction, Coulomb failure, and the fluid-solid transition for horizontally shaken granular materials. *Phys Rev E Stat Phys Plasmas Fluids Relat Interdiscip Topics*. 2002;65(3):1-15.
24. Liffman K, Metcalfe G, Cleary P. Granular convection and transport due to horizontal shaking. *Phys Rev Lett*. 1997;79(23):4574-4576.
25. Shimamoto A, Kodama M, Yamamura M. Vibration tests for scale model of cylindrical coal storing silo. 1984;5:287-294.
26. Yokota H, Sugita M, Mita I. Vibration tests and analyses of coal-silo model. In Proc., 2nd Int. Conf. on the Design of Silos for Strength and Flow, Stratford-upon-Avon, Powder Advisory Centre, 1983; pp. 107-116.
27. Chandrasekaran AR, Jain PC. Effective live load of storage materials under dynamic conditions. *Indian Concr J*. 1968;42(9):364-365.
28. Chandrasekaran AR, Saini SS. Live load effect on dynamic response of structures. *J Struct Div*. 1968;95(4):649-660.
29. Lee SJ. Experimental study of cylindrical silos subject to seismic excitation. 1981. Doctoral dissertation, The Ohio State University.
30. Harris EC, Von Nad JD. Experimental determination of effective weight of stored material for use in seismic design of silos. *ACI J Proc*. 1985;82(6).
31. Sasaki Y & Yoshimura J Dynamic behavior of concrete stave silos. Proceedings of the 8th World Conference on Earthquake Engineering, San Francisco, USA, 1984;5:287-294.
32. Sasaki Y & Yoshimura J Seismic response of concrete stave silos with structural discontinuity. Proceedings of the 9th World Conference on Earthquake Engineering, Tokyo-Kyoto, 1988; Vol. VI.
33. Tatko R, Kobiela S. Horizontal Bulk Material Pressure in Silo Subjected to Impulsive Load. *Shock and Vibration*. 2008;15(5):543-550.
34. Peloso S, Pavese A, Casarotti C, Eucentre trees lab: laboratory for training and research in earthquake engineering and seismology. *Geotech Geol Eng Earthq Eng*. 2012;20: 65-81.
35. Pavese A, Furinghetti M, Casarotti C. Investigation of the consequences of mounting laying defects for curved surface slider devices under general seismic input. *J Earthq Eng*. 2019; 23(3): 377-403.
36. Furinghetti M, Pavese A, Quaglini V, Dubini P. Experimental investigation of the cyclic response of double curved surface sliders subjected to radial and bidirectional sliding motions. *Soil Dyn Earthq Eng*. 2019;117:190-202.
37. Tang G, Sun P, Zhao Y, Yin L, Zhuang H. Experimental research on friction coefficient between grain bulk and bamboo clappers. *IOP Conf Ser: Mater Sci*. 2017; 274(1): 012116.
38. Code for design of grain steel silos, Beijing, GB 50322-52011
39. Sadowski AJ, Rotter JM. Buckling of very slender metal silos under eccentric discharge. *Eng Struct*. 2011;33:1187-1194.
40. Allen RL, Mills D. *Signal Analysis: Time, Frequency, Scale, and Structure*. John Wiley & Sons; 2004.
41. Chopra AK. *Dynamics of Structures. Theory and Applications to Earthquake Engineering*. Upper Saddle River: Prentice-Hall; 2001.

How to cite this article: Silvestri S, Mansour S, Marra M, et al. Shaking table tests of a full-scale flat-bottom manufactured steel silo filled with wheat: Main results on the fixed-base configuration. *Earthquake Engng Struct Dyn*. 2022;51:169-190. <https://doi.org/10.1002/eqe.3561>